Editors' Suggestion   Featured in Physics

Flow Rectification in Loopy Network Models of Bird Lungs

Quynh M. Nguyen [1,2] Anand U. Oza [3] Joanna Abouezzi,[1] Guanhua Sun,[1] Stephen Childress [1]
Christina Frederick [3] and Leif Ristroph[1,*]

[1]*Applied Math Lab, Courant Institute, New York University, New York, New York 10012, USA*
[2]*Physics Department, New York University, New York, New York 10003, USA*
[3]*Department of Mathematical Sciences, New Jersey Institute of Technology, Newark, New Jersey 07102, USA*

We demonstrate flow rectification, valveless pumping, or alternating to direct current (AC-to-DC) conversion in macroscale fluidic networks with loops. Inspired by the unique anatomy of bird lungs and the phenomenon of directed airflow throughout the respiration cycle, we hypothesize, test, and validate that multiloop networks exhibit persistent circulation or DC flows when subject to oscillatory or AC forcing at high Reynolds numbers. Experiments reveal that disproportionately stronger circulation is generated for higher frequencies and amplitudes of the imposed oscillations, and this nonlinear response is corroborated by numerical simulations. Visualizations show that flow separation and vortex shedding at network junctions serve the valving function of directing current with appropriate timing in the oscillation cycle. These findings suggest strategies for controlling inertial flows through network topology and junction connectivity.

Oscillatory, random or otherwise undirected movements can be induced into progressive motion by the presence of asymmetries. Rectification of fluids is a form of pumping [1–5], which is conventionally achieved via valves whose opening and closing motions are biased to direct flows appropriately. For example, the circulatory system involves pulsations produced by the beating heart that are rectified by flaplike valves to drive directed flow of blood through vessels. It is interesting and potentially useful that such alternating to direct current (AC-to-DC) conversion of flows can also be achieved without moving elements but instead with entirely static geometries. This is permissible due to fluid dynamical irreversibility at high Reynolds numbers, for which the dominance of inertia over viscosity leads to phenomena such as flow separation and vortex shedding that respond sensitively to geometry and thus directionality [6,7]. Such effects are exploited in fluidic diodes, devices whose asymmetric internal geometries lead to direction-dependent hydraulic resistance. Examples include conduits with diverging or converging walls, sawtoothed corrugations, and more complex geometries proposed by Tesla and others [4,8–10].

Here we explore an alternative strategy for flow rectification in which the topology and connectivity of a network of symmetric pipes or channels leads to persistent circulation in response to oscillatory forcing. Our inspiration comes from a remarkable physiological observation: While air flow in the lungs of mammals oscillates with inhalation and exhalation, directional flows throughout the respiration cycle have been measured in birds [11–18]. This flow pattern may contribute to respiratory efficiency and has been viewed as an adaptation for the high metabolic

demands of flight, although recent discoveries in reptiles suggest that the trait is ancestral [19–21]. The bird lung differs fundamentally from that of mammals in that its conduits are not only branched but also *reconnect* to form *loops* [12,22,23]. Indeed, the directed flows are observed along looped airways formed by dorso-, para-, and ventrobronchi (DPV), as illustrated in the anatomical schematic of Fig. 1(a). This respiratory network is thus broadly analogous to a circulatory system, with alternating or AC forcing via air sac (AS) contraction and expansion driving directional or DC flows around loops [12,15]. However, no valvular structures have been found in bird lungs [23,24], spurring various hypotheses for rectification that invoke static bafflelike structures that "guide" flows [12], bronchial tube constrictions and divergences that induce separated flows and jets [25–28], the curvature of tubes and their angles at junctions [29,30], and phased expansion or contraction of multiple air sacs and their compliance [31,32]. Importantly, the Reynolds numbers Re ∼ 100–1000 are high [14,33,34], and studies that vary gas density and flow speed indicate the importance of inertial effects [34,35]. In particular, studies by Banzett and co-workers on anesthetized birds point to an inherently aerodynamic source of valving in which inertia or momentum directs flows at junctions [25,26,33,35,36].

Building on these works, here we test and verify that loopy networks driven with oscillations or pulsations at high Reynolds numbers represent sufficient ingredients for AC-to-DC conversion. Toward isolating the physical factors essential for rectification, we begin with a series of geometrical idealizations of the avian respiratory network. In Fig. 1(b) we show a "spherical bird"
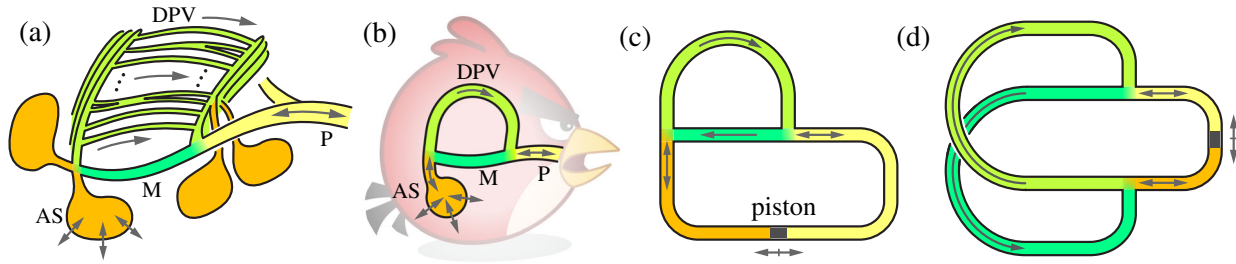
FIG. 1. Loopy network models of bird lungs. (a) Schematic of anatomy modified from Ref. [11]. Reciprocal expansion and contraction of air sacs (AS) drives oscillatory inhalation and exhalation flows in the primary bronchus (P). Directed flow is observed in dorso-, para-, ventrobronchi (DPV) that span the mesobronchus (M). (b) A "spherical bird" simplification with a single AS and DPV. (c) A closed network formed by connecting P to AS, the latter replaced by a reciprocating piston. (d) A symmetrized network that modifies conduit lengths while preserving the connectivity of the T junctions.

approximation that isolates one DPV arc, which connects to a single caudal air sac on one end and to the primary bronchus (P) on the other, the latter idealized as a tube that opens to the outside at the mouth. A closed loop is formed by DPV and the mesobronchus (M). The air sac functions as a bellows that reciprocally expands and contracts to drive inspiration and expiration. The system is transformed into a closed circuit by replacing the air sac with a reciprocating piston and rerouting the main bronchus to attach as shown in Fig. 1(c). This closure is an experimental and computational convenience for studying flows internal to the network and without regard to exchange with the external environment.

Laboratory demonstrations prove the rectification capability of the circuit of Fig. 1(c), as shown in Video 1 in the Supplemental Material [37]. A system is constructed from clear rubber tubing and T-junction fittings, filled with water and flow-tracing particles, and driven via a reciprocating roller that serves the function of a piston. While the flow in the lower portion (yellow and orange) matches the driving motions and is purely AC, the upper segment (light green) displays directed or DC flows. Their sense is indicated by the arrow in Fig. 1(c) and matches that observed in the DPV of bird lungs. Further, DC motions are apparent in the straight segment (dark green, M) connecting the two junctions. In essence, circulation develops around the closed loop that includes DPV and M, and the system acts as a circulating pump, fluidic rectifier, or AC-to-DC converter.

The network of Fig. 1(c) contains asymmetries not critical to rectification, as demonstrated by considering further transformations that result in the symmetrized circuit of Fig. 1(d). The lengths and trajectories of the conduits are manipulated while preserving the network topology, junction geometry, and connectivity. Specifically, the side branch of each T junction feeds into the straight segment of the partner junction. This can be achieved in various 3D arrangements and in the quasi-2D layout of Fig. 1(d), which is planar except for a slight defect where the conduits cross. Demonstrations again show persistent DC circulation for AC driving. The network is mirror symmetric and so are the

time-averaged DC flows, which emanate from the straight branches and return through the side branches of the junctions, as indicated in Fig. 1(d). These observations rule out an explanation of the observed rectification based on spontaneous symmetry breaking.

More careful experiments show that the rectified flows are reproducible for given forcing parameters and vary systematically with these parameters. As shown in the experimental schematic of Fig. 2(a), a version of the symmetric system is constructed from rigid tubing and custom-made junctions (all of uniform inner diameter $D = 1.6$ cm), filled with water, and connected to a motorized piston that oscillates sinusoidally with controllable amplitude $A \sim 0.3$–8 cm and frequency $f \sim 0.3$–3 Hz. This yields high Reynolds numbers that span those relevant to bird respiration [14,33,34]: $\mathrm{Re} = \rho A f D / \mu \sim 10$–5000, where $\rho = 1.0$ g/cm^3 and $\mu = 8.9 \times 10^{-3}$ dyn $\cdot$ s/cm^2 are the density and viscosity of water, respectively. Seeding with microparticles allows for flow measurement via particle image velocimetry (PIV). A portion of the pipe in one of the DC branches is illuminated by a laser sheet and imaged with a high-speed camera, and a rectangular water jacket and thin-walled tubing ensure minimal optical distortion. The measured particle motions yield time- and space-resolved flow velocity fields. Profiles of the axially averaged velocity, sampled throughout an oscillation period, are shown in Fig. 2(b) for selected values of A and f. Rectification manifests as a bias toward positive velocities. Assuming that the flow is axisymmetric, the radial average of the flow velocity yields the section-averaged speed shown in Fig. 2(c). Its time average U quantifies the emergent DC flow speed or, equivalently, the time- and section-averaged volumetric flux (volume flow rate per unit area).

The performance as an AC-to-DC converter can be characterized by measuring the output U across different values for the input parameters A and f. The plots of Fig. 3(a) show systematic trends in these data, and repeated measurements at each A and f indicate reproducibility of the phenomenon and reliability of the measurements.
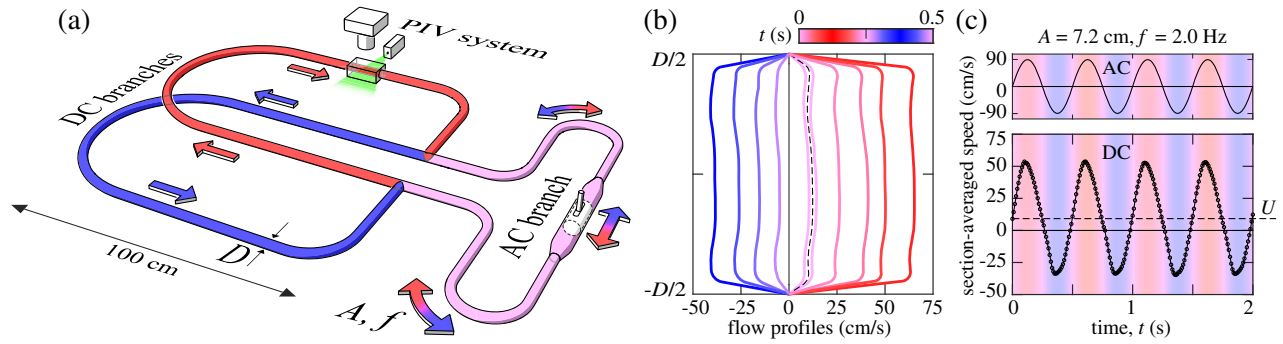
FIG. 2. Experimental system for characterizing flows in a forced fluidic network. (a) Rigid tubing of inner diameter $D = 1.6$ cm is formed and connected via T junctions, and the network is filled with water seeded with microparticles. Oscillatory flow in the AC branch is driven by a motorized piston that oscillates with amplitude A and frequency f, and the resulting flow field in a DC branch is measured via PIV. (b) Flow profiles in the DC branch measured at different times in the cycle for $A = 7.2$ cm and $f = 2.0$ Hz ($A/D = 4.5$, $\text{Wo}^2 = 900$, and $\text{Re} = 2500$). Rectification is evident as the positive bias in the time-averaged profile (dashed curve). (c) Imposed oscillatory flow in the AC branch (top) and measured section-averaged flow in a DC branch (bottom); the time average U of the latter characterizes the pump rate.

The pump rate increases with A and f for all but the smallest values of these parameters, for which U is small or even negative (inset).

A dimensionless measure of pumping effectiveness is $E = U/2Af$, which compares the output DC speed to the characteristic input AC speed. Quantitatively, $E = 1$ represents perfect rectification in the following sense. A stroke of the piston in one direction, say the downward motion marked in red in Fig. 2(a), displaces fluid in the AC branch by an amount $2A$ in the duration $1/2f$. The entire flux $4Af$ is injected straight past the lower T junction and into the DC branch colored red, and it returns in whole to the other side of the AC branch by turning at the upper junction. The side branch of the lower junction behaves as if sealed shut by a valve, deactivating the other DC branch (blue). The DC branches and T junctions swap roles in the return stroke. This ideal behavior is thus half-wave rectification with cycle-averaged flux $U = 2Af$ in each DC branch; hence $E = 1$. Figure 3(b) shows the measured $E(A, f)$ to be as high as 0.4, and the trends indicate increasing E for greater A and f.

The normalization $E = U/2Af$ fails to collapse these data, highlighting the nonlinear response of the system. A fully dimensionless characterization can be formed in terms of A/D, which represents the oscillatory amplitude relative to conduit diameter, and the square of the Womersley number $\text{Wo}^2 = \pi\rho f D^2/2\mu$, which is proportional to f and assesses the unsteadiness of pulsatile flow [38]. Figure 3(c) displays $E(A/D, \text{Wo}^2)$, showing increasingly effective pumping in both driving parameters. Also shown are the hyperbolic contours of the Reynolds number $\text{Re} = (2/\pi)(A/D)\text{Wo}^2$.

To further validate these findings, we implement computational fluid dynamics simulations relevant to the asymmetric circuit of Fig. 1(c). The two-dimensional Navier-Stokes equation for incompressible flow is numerically solved using the finite element method in the domain defined in Fig. 4(a), where no-slip boundary conditions are imposed on the static walls as well as the reciprocating piston, the neighborhood of which is treated using an Arbitrary Lagrangian-Eulerian (ALE) formulation [39]. The simulations are carried out using the COMSOL Multiphysics software package with laminar flow settings [40]. A detail of the spatial grid near one T junction is shown in the inset. The system parameters span the ranges $A/D \sim 0.1$–10, $\text{Wo}^2 \sim 10$–200, and $\text{Re} \sim 10$–1000. Compared to our experiments, the simulations are restricted to lower Wo^2 but permit larger A/D, leading to comparable Re. Additional implementation details are available in Supplemental Material [37].

We assess the dependence of the terminal or longtime mean flow rate U on the driving parameters A and f. Our results reproduce all phenomenology and trends seen in experiments, as shown by the $E(A/D, \text{Wo}^2)$ map in Fig. 4(b) and the associated curves in the Supplemental Material [37]. The simulations typically yield values of E that are several times greater than those measured at corresponding conditions in experiments. This may be attributed to dimensionality (2D simulations versus 3D experiments), the use of asymmetric versus symmetric forms of the circuit, and the consequent differences in the lengths and curvatures of the conduits. These factors affect the resistance of DPV and M, and the longer conduits used in experiments and thus higher resistance may contribute to the lower effectiveness. Nonetheless, the features of emergent DC flows, their sense of direction, and qualitative trends for varying driving parameters are robust to these geometric differences. The maps of Figs. 3(c) and 4(b) indicate that, for large Re, contours of constant Re roughly correspond to constant E, suggesting that extrapolation may be used to estimate E for values of A/D and Wo^2 larger than those explored here.
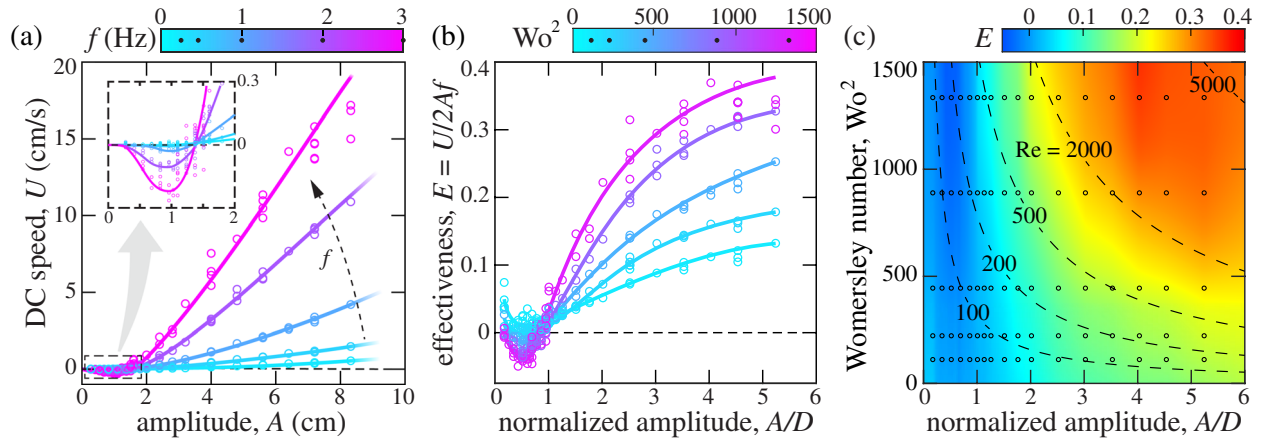
FIG. 3. Experimental characterization of AC-to-DC conversion in the symmetric circuit of Fig. 2. (a) Dependence of DC flow speed U on AC driving parameters A and f. Multiple data points represent independent trials, Bezier curves are shown as guides to the eye, and values of f are indicated on the color bar. Inset: magnified view of low-A data. (b) Effectiveness $E = U/2Af$ as a dimensionless measure of AC-to-DC conversion. (c) Map of E across normalized amplitude A/D and frequency $Wo^2 \propto f$. Markers indicate where measurements are performed, and the map is generated by linear interpolation or extrapolation and smoothing via moving-window averaging.

The simulations provide access to the flow fields, as shown in Videos 2 and 3 in Supplemental Material [37], and thereby offer insight into the rectification mechanism. In Fig. 4(c) we focus on streamlines and vorticity near the junction highlighted in Fig. 4(a) and at four instances in the oscillation cycle. At peak velocity during inhalation (first image), fluid is injected from P and predominantly goes straight past the junction down M, with little turning up DPV. This matches the intuition that inertia of the flow tends to maintain its straight course. A stagnation streamline impinges on the far (left) corner of the junction and divides the straight and turning flows, and a large vortex shed from the near (right) corner "plugs" the side branch. At peak velocity during exhalation (third image), fluid exits

the junction via P and draws more equally from M and DPV. The converging currents are divided by a separation streamline emanating from the far corner, and vorticity produced at the near corner does not detach but rather "hugs" the wall of P. Integrating in time over a cycle, the indicated junction thus has net flux incoming from the side branch (DPV) and exiting via the straight branch (M), which corresponds to net circulation in the clockwise sense around the DPV-M loop. Consistent with mass conservation, the other junction also has net flux entering via its side branch and exiting via the straight branch, these associated with M and DPV, respectively. In essence, flow separation and vortex shedding serve the valving function of closing and opening the side branch with appropriate timing in the
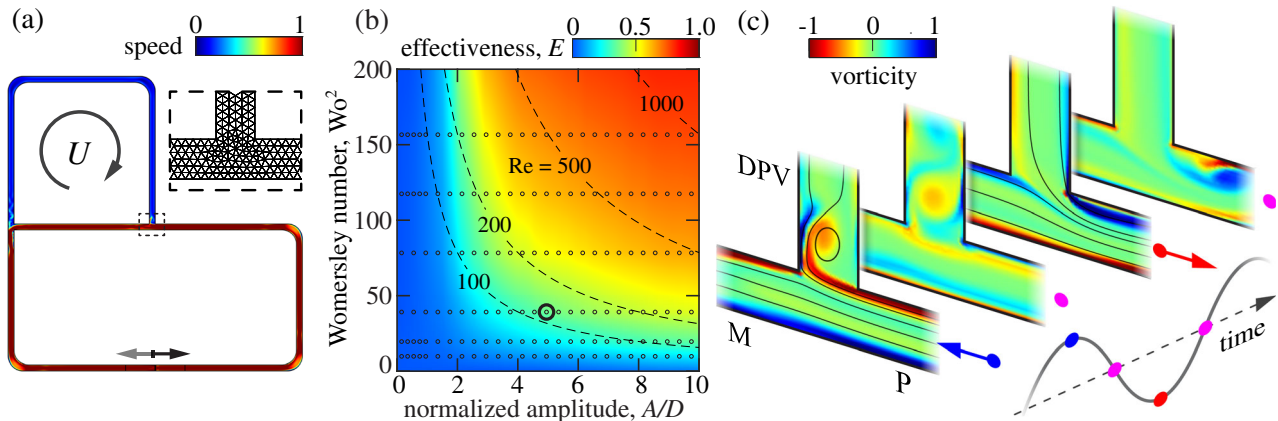

FIG. 4. Simulation of the asymmetric circuit. (a) The domain and spatial grid near a T junction (inset). Color indicates flow speed normalized by $2\pi fA$ and at the moment the piston is moving rightward at peak velocity. Here $D = 0.5$ cm, $A = 2.5$ cm, and $f = 1$ Hz. (b) Effectiveness E across A/D and $Wo^2 \propto f$. (c) Streamlines and vorticity near one junction at four equally spaced phases in the cycle and for the parameters circled in (b). Arrows indicate the phase of the imposed flow from the primary bronchus (P). Vorticity is normalized by $\pi^2 f(A/D)^2$, a scale appropriate for vortex shedding from a sharp edge in oscillatory flow [41,42].

cycle. Analogous phenomena are expected to occur in 3D settings, which could be assessed through flow visualization and quantification in experiments as well as 3D simulations.

These results complement the physiological studies by Banzett and others on the aerodynamic origins of valving in birds during inspiration [25,26,33,35,36] by providing realizations of driven networks in physical experiments and simulations. We have demonstrated the unsteady and separated nature of the causal flows at junctions and characterized the consequent nonlinear response over relevant fluid dynamical parameters. Taken together, these results establish a form of fluidic rectification that is ultimately rooted in kinematic irreversibility at high Reynolds numbers [6,7], which plays an analogous role in contexts such as expulsion versus suction from orifices and reverse versus forward flow through asymmetric conduits. The relevant asymmetry in our system is more subtle: Each T junction has an axis of symmetry, but its anisotropic shape has distinct straight and side branches with differing end conditions due to their connectivity to the partner junction. Rectified flows of the type observed here are impossible for $\mathrm{Re} = 0$ or viscous-dominated conditions, for which the governing Stokes equation is reversible and the scallop theorem ensures flows induced in one stroke are retraced reversely in the return stroke [6,43]. Rectification is also precluded in the other extreme of inviscid and irrotational flow due to Kelvin's circulation theorem [6]. Hence, the valving mechanism described here may operate at any finite Re, though it is expected to be exceedingly weak for $\mathrm{Re} < 10$. The turbulent flow regime of $\mathrm{Re} > 2000$, while less relevant to bird lungs, may be applicable to other problems and awaits future studies.

The phenomena reported here may arise more generally in the looped topologies common across many biological and physiological flow networks, which are often subject to unsteady forcing and pulsatile flows [44,45]. Loops play the essential role of providing routes around which circulation can be established. Our systems are minimal in that they comprise two interconnected loops, one whose AC flow is prescribed and the other free to display an emergent DC flow. Loops necessitate junctions, and the mechanism described above suggests that their geometrical anisotropy is critical. We posit that any anisotropy, appropriately mirrored for partner junctions, will in general induce rectification. In this sense, the T shape used here is not critical, and the complexities of junction flows invite optimization over parameters such as branching angles [36,46–49]. Future studies might vary not only the junction and conduit geometries but also the driving waveform and global network topology and connectivity, which could further inform on respiration phenomena and flow transport in complex networks generally. The value of the simpler circuits studied here is in identifying loops, anisotropic junctions, and inertial flows as sufficient ingredients for rectification.

[*]ristroph@cims.nyu.edu

[1] A. Glezer and M. Amitay, Annu. Rev. Fluid Mech. **34**, 503 (2002).
[2] M. Prakash, D. Quéré, and J. W. M. Bush, Science **320**, 931 (2008).
[3] G. Lagubeau, M. Le Merrer, C. Clanet, and D. Quéré, Nat. Phys. **7**, 395 (2011).
[4] B. Thiria and J. Zhang, Appl. Phys. Lett. **106**, 054106 (2015).
[5] J. Mo, C. Li, L. Li, J. Wang, and Z. Li, Phys. Fluids **28**, 082005 (2016).
[6] D. J. Tritton, *Physical Fluid Dynamics* (Springer Science & Business Media, New York, 2012).
[7] H. Schlichting and K. Gersten, *Boundary Layer Theory* (Springer, New York, 2016).
[8] N. Tesla, Valvular conduit, U. S. Patent No. 1,329,559 (3,2,1920).
[9] A. Groisman and S. R. Quake, Phys. Rev. Lett. **92**, 094501 (2004).
[10] R. Tao, T. Ng, Y. Su, and Z. Li, Phys. Fluids **32**, 052010 (2020).
[11] P. Scheid, H. Slama, and J. Piiper, Respir. Physiol. **14**, 83 (1972).
[12] E. Hazelhoff, Poult. Sci. **30**, 3 (1951).
[13] J. Cohn and R. Shannon, Respir. Physiol. **5**, 259 (1968).
[14] W. L. Bretz and K. Schmidt-Nielsen, J. Exp. Biol. **54**, 103 (1971).
[15] J. H. Brackenbury, Respir. Physiol. **13**, 319 (1971).
[16] F. Powell, J. Geiser, R. Gratz, and P. Scheid, Respir. Physiol. **44**, 195 (1981).
[17] J. N. Maina, Biol. Rev. Camb. Philos. Soc. **92**, 1475 (2017).
[18] J. H. Jones, E. Effmann, and K. Schmidt-Nielsen, Respir. Physiol. **45**, 121 (1981).
[19] C. Farmer and K. Sanders, Science **327**, 338 (2010).
[20] E. R. Schachner, R. L. Cieri, J. P. Butler, and C. Farmer, Nature (London) **506**, 367 (2014).
[21] R. L. Cieri and C. Farmer, J. Comp. Physiol. B **186**, 541 (2016).
[22] P. Biggs and A. King, J. Physiol. **138**, 282 (1957).
[23] H. Duncker, Respir. Physiol. **22**, 1 (1974).
[24] A. S. King and D. C. Payne, J. Anat. **96**, 495 (1962).
[25] R. B. Banzett, C. S. Nations, N. Wang, J. J. Fredberg, and J. P. Butler, Respir. Physiol. **84**, 295 (1991).
[26] N. Wang, R. B. Banzett, C. S. Nations, and F. A. Jenkins Jr, J. Exp. Zool. **262**, 441 (1992).
[27] J. N. Maina and M. Africa, J. Exp. Biol. **203**, 2865 (2000).
[28] E. Sakai, T. Watanabe, and T. Himeno, J. Mech. Med. Biol. **6**, 299 (2006).
[29] J. H. Brackenbury, Respir. Physiol. **15**, 384 (1972).
[30] J. Maina, P. Singh, and E. Moss, Respir. Physiolo. Neurobio. **169**, 262 (2009).

[31] A. Urushikubo, M. Nakamura, and H. Hirahara, J. Biomed. Sci. Eng. **6**, 483 (2013).

[32] E. P. Harvey and A. Ben-Tal, PLoS Comput. Biol. **12**, e1004637 (2016).

[33] J. P. Butler, R. B. Banzett, and J. J. Fredberg, Respir. Physiol. **72**, 241 (1988).

[34] D. O. Kuethe, J. Exp. Biol. **136**, 1 (1988).

[35] R. B. Banzett, J. P. Butler, C. S. Nations, G. M. Barnas, J. L. Lehr, and J. H. Jones, Respir. Physiol. **70**, 287 (1987).

[36] N. Wang, R. B. Banzett, J. P. Butler, and J. J. Fredberg, Respir. Physiol. **73**, 111 (1988).

[37] See Supplemental Material at http://link.aps.org/supplemental/10.1103/PhysRevLett.126.114501 for additional details of the simulations and supporting data.

[38] J. R. Womersley, J. Physiol. **127**, 553 (1955).

[39] C. W. Hirt, A. A. Amsden, and J. Cook, J. Comput. Phys. **14**, 227 (1974).

[40] COMSOL Multiphysics® v. 5.4, https://www.comsol.com.

[41] T. Schnipper, A. Andersen, and T. Bohr, J. Fluid Mech. **633**, 411 (2009).

[42] N. Agre, S. Childress, J. Zhang, and L. Ristroph, Phys. Rev. Fluids **1**, 033202 (2016).

[43] E. M. Purcell, Am. J. Phys. **45**, 3 (1977).

[44] K. Schmidt-Nielsen, *Animal Physiology: Adaptation and Environment* (Cambridge University Press, Cambridge, England, 1997).

[45] Y. Fung, *Biomechanics: Circulation* (Springer Science & Business Media, 2013).

[46] J. T. Ault, A. Fani, K. K. Chen, S. Shin, F. Gallaire, and H. A. Stone, Phys. Rev. Lett. **117**, 084501 (2016).

[47] S. Takagi and K. Takahashi, Bull. JSME **28**, 831 (1985).

[48] F. Haselton and P. Scherer, J. Fluid Mech. **123**, 315 (1982).

[49] B. Mauroy, M. Filoche, J. S. Andrade, and B. Sapoval, Phys. Rev. Lett. **90**, 148101 (2003).

Supplemental Material for "Flow rectification in loopy network models of bird lungs"

Quynh M. Nguyen,[1,2] Anand U. Oza,[3] Joanna Abouezzi,[1] Guanhua Sun,[1] Stephen Childress,[1] Christina Frederick,[3] and Leif Ristroph[1]

[1] *Applied Math Lab, Courant Institute of Mathematical Sciences,*
New York University, New York, New York 10012, USA
[2] *Physics Department, New York University, New York, New York 10003, USA*
[3] *Department of Mathematical Sciences, New Jersey Institute of Technology, Newark, New Jersey 07102, USA*
(Dated: February 19, 2021)

NUMERICAL SIMULATIONS

The incompressible Navier-Stokes equations are solved numerically in the two-dimensional domain shown in Fig. 1:

$$\rho \left(\frac{\partial \boldsymbol{u}}{\partial t} + \boldsymbol{u} \cdot \boldsymbol{\nabla} \boldsymbol{u} \right) = -\boldsymbol{\nabla} p + \mu \Delta \boldsymbol{u},$$
$$\boldsymbol{\nabla} \cdot \boldsymbol{u} = 0, \tag{1}$$

where $\boldsymbol{u} = \boldsymbol{u}(\boldsymbol{x}, t) \in \mathbb{R}^2$ is the fluid velocity field, $p = p(\boldsymbol{x}, t) \in \mathbb{R}$ is the pressure, and $\rho = 1.0$ g/cm^3 and $\mu = 8.9 \times 10^{-3}$ g/(cm·s) are, respectively, the density and dynamic viscosity of water. We assume the fluid to start at rest and thus impose the initial conditions $\boldsymbol{u}(\boldsymbol{x}, 0) = 0$ and $p(\boldsymbol{x}, 0) = 0$. The oscillatory motion of a piston is given by $x_p(t) = A \cos 2\pi f t$, where A and f are the forcing amplitude and frequency, respectively. No-slip conditions are imposed on all boundaries; specifically, $\boldsymbol{u} = 0$ on the walls, and $\boldsymbol{u} = (\dot{x}_p, 0)$ on the boundary of the piston. The piston has width $l = D/10$, where $D = 0.5$ cm is the pipe diameter. The corners in the domain, with the exception of the two T-junctions, are rounded with a radius of curvature $L/20$.

The equations are solved numerically by the finite element method using COMSOL Multiphysics®. The fluid velocity $\boldsymbol{u}$ is approximated by piecewise quadratic functions (P2), and the pressure p by piecewise linear functions (P1), so as to satisfy the Ladyženskaja-Babuška-Brezzi (LBB) condition. A free triangular mesh is used throughout most of the domain (Fig. 1, top inset), and the maximum element size is $D/5$. In a neighborhood of the moving piston, we use an Arbitrary Lagrangian-Eulerian (ALE) formulation [1] to solve the PDE on time-dependent mesh points. The mesh is fixed in terms of the ALE coordinates (X, Y), which identify points in a fixed reference domain corresponding to the colored regions in Fig. 1 (lower inset). These regions are discretized using a mapped mesh, in which the elements are split by inserting diagonal edges. In the domains to the left (red, $-$) and right (blue, $+$) of the piston, the ALE coordinates are related to the physical coordinates $(x_\pm(t), y)$ by the formula $x_\pm(t) = X + x_p(t)(A + l \mp X)/(A + l/2)$. Note that $y = Y$ because the piston does not move vertically.
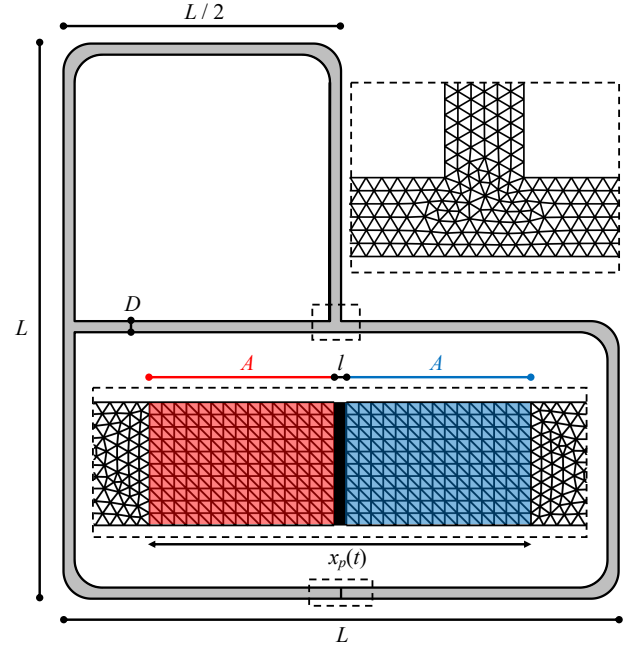

FIG. 1. The Navier-Stokes equations are solved in the gray region shown in the figure. The top inset shows the mesh near a junction, and the bottom inset shows the mesh around the piston (black region).

The simulations are performed for a maximum time $t_{\max} = 20T$, where $T = 1/f$ is the forcing period. The effectiveness $E = U/2Af$ is computed by averaging the flux in the DC loop over the last forcing cycle:

$$U = \frac{1}{DT} \int_{t_{\max}-T}^{t_{\max}} dt \int_D d\boldsymbol{x} \, u(\boldsymbol{x}, t) \tag{2}$$

where $\int_D$ denotes an integral over the pipe diameter within the DC loop. Both integrals are computed using trapezoidal rule. Computing the flux along different pipe sections in the DC loop gives consistent results. For example, for the simulations shown in Fig. 4(c) of the Main Text, the values of E computed along each of the four sides of the DC loop differ by less than 10^{-5}.

SUPPORTING DATA

The dependence of the effectiveness E on both the Womersley number Wo and amplitude A is shown in Fig. 2(a). The simulation results are largely unchanged upon refinement of the mesh. Specifically, all of the data points were re-computed with a more refined mesh, with a maximum element size of $D/10$. The maximum difference in the effectiveness between the coarse and refined simulations is $\Delta E = 0.1$, and the average difference is $\Delta E = 0.02$.

Figures 2(b) and 2(c) show the dependence of the effectiveness on Wo and the Reynolds number Re from simulations and experiments, respectively, as obtained by recasting the data in panel (a) and Fig. 3(b) of the Main Text. The curves from simulations in panel (b) appear to overlap at high Re. This indicates that, in the limit of high Re, the effectiveness $E = E(A/D, \mathrm{Wo}^2)$ is largely dependent not separately on A/D and Wo^2 but on their product, which is proportional to Re.
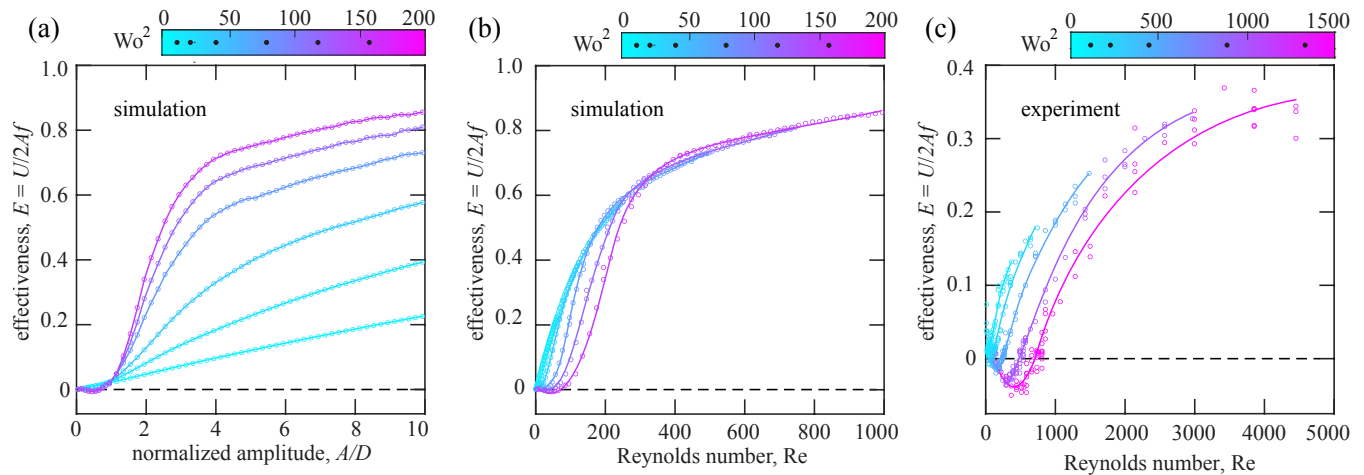

FIG. 2. (a) Simulation data showing the dependence of the effectiveness E on the dimensionless forcing amplitude A/D and Womersley number Wo, the latter indicated by the black dots in the colorbar. The data are identical to that reported in Fig. 4(b) of the Main Text. (b) Simulation data from panel (a), recast to show the dependence of E on the Reynolds number Re and Wo. (c) Experimental data showing the dependence of E on Re and Wo. The data are identical to that reported in Fig. 3(b) of the Main Text. In panels (b) and (c), Bezier curves are shown as guides to the eye.

[1] C. W. Hirt, A. A. Amsden, and J. L. Cook, J. Comp. Phys. **14**, 227 (1974).
[2] T. Schnipper, A. Andersen, and T. Bohr, J. Fluid Mech. **633**, 411 (2009).

SUPPLEMENTAL VIDEO CAPTIONS

VIDEO 1

This video visualizes experiments of flow rectification in a two-loop network. Clear rubber tubes of inner diameter $D = 1$ cm are connected by two T-junction fittings. The closed circuit is filled with water, and cotton balls are used as flow tracers. A reciprocating roller completely pinches shut and forces AC flow in the lower branch, as indicated by the tracers oscillating in place. DC flow emerges in the upper branch, as indicated by the clockwise motions of the tracers. The roller oscillates with frequency $f = 1.4$ Hz and amplitude $A = 2$ cm.

VIDEO 2

The video shows the dimensionless vorticity ω/ω_0, where $\omega = \boldsymbol{\nabla} \times \boldsymbol{u}$ and $\omega_0 = \Gamma_0/D^2$. Here, $\boldsymbol{u}$ is the flow velocity, D is the pipe diameter and $\Gamma_0 = \int_0^{1/(2f)} \dot{x}_p(t)^2 \, \mathrm{d}t = \pi^2 A^2 f$ is an estimate [2] for the circulation shed from a sharp corner in an oscillatory flow with velocity $\dot{x}_p$, where $x_p(t) = A \cos 2\pi f t$ is the position of the piston. The forcing amplitude is $A/D = 5$ and frequency $f = 1$ Hz, corresponding to the square of the Womersley number $\mathrm{Wo}^2 = 39$. The regions near the two T-junctions are magnified in the insets.

VIDEO 3

The video shows the flow speed $|\boldsymbol{u}|/u_0$ (color) and direction $\boldsymbol{u}/|\boldsymbol{u}|$ (arrows), where $\boldsymbol{u}$ is the flow velocity and $u_0 = 2\pi f A$ the peak speed of the piston. The simulation parameters are the same as those in Supplemental Video 2.